Available online at www.sciencedirect.com
SCIENCE DIRECT®
Catalysis Today 97 (2004) 195–203
CATALYSIS TODAY
www.elsevier.com/locate/cattod

Single-step preparation of Ni catalysts supported on mesoporous silicas (SBA-15 and SBA-16) and the effect of pore structure on the selective hydrodechlorination of 1,1,2-trichloroethane to VCM

Younggeun Park, Taewook Kang, Jaeho Lee, Pil Kim, Heesoo Kim, Jongheop Yi*

School of Chemical Engineering, Seoul National University, San 56-1, Shillimdong, Kwankgu, Seoul, Korea

Received 18 November 2003; received in revised form 8 March 2004; accepted 20 March 2004
Available online 11 September 2004

Abstract

A nickel catalyst supported on mesoporous silica was synthesized using a single-step sol–gel scheme with a triblock copolymer as the structure-directing agent. The role of the surfactant is to organize the silica into the highly ordered 2D hexagonal and 3D cubic structure, via an ionic assembly pathway. The addition of Ni^{2+} ions to the solution results in a strong interaction between the head group (polyethylene oxide, PEO), Ni^{2+} ions, and the silica precursors (tetraethoxysilane, TEOS). PEO is exposed to hydrophilic conditions in acidic media, and consequently combines with nickel ions by electrostatic force. Thus, the nickel particles are located on the surface of the mesostrucutre, within the mesoporous and outer surface. After calcination, the catalysts had a small and regular size metal dispersion with a well-defined cylindrical pore structure and a narrow pore size distribution, as evidenced by XRD, TEM, N_2 adsorption, ICP-AES, and EXAFS. Using the SBA-16 type support with 3D cage like, mesopore structure and a high micropore ratio, the hydrodechlorination of 1,1,2-trichloroethane was found to be relatively efficient. Moreover, high VCM selectivity could be obtained on nickel catalysts prepared via the single-step method.
© 2004 Elsevier B.V. All rights reserved.

Keywords: Single step; Mesoporous silica; SBA-15; SBA-16; Hydrodechlorination; 1,1,2-Trichlroethane; Vinyl chloride monomer

1. Introduction

Chlorinated hydrocarbon compounds represent undesirable byproducts that are produced during petroleum refining and in the pharmaceutical industry, and are highly toxic to the environment. Thus, it is necessary to develop an efficient detoxification process. Catalytic hydrodechlorination [1] is more desirable than other methods such as incineration [2], biological treatment [3] and photo-catalytic decomposition [4]. In addition to contributing to a cleaner environment, this process has clear economic merits due to the fact that the resulting hydrocarbons can be recovered and recycled. One example is the production of vinyl chloride monomer from waste chlorinated hydrocarbons. As opposed to the large body of data concerning catalytic hydrodechlorination, little information is available concerning more complex polychlorinated aromatic compounds, such as the reaction of hydrogen with chlorobenzene [5].

In order to reduce or diminish bulky chlorinated hydrocarbons, a high surface area and large pore volume with an ordered structure are required to improve catalytic performance. As a result, considerable interest has developed in the synthesis of mesostructured materials composed of organic and inorganic frameworks. The use of micellar aggregates of long chain organic surfactant molecules as a template to direct and control the structure of the silicate network has proven to be partially successful for tailor-made mesoporous materials such as MCM-41, MCM-48, SBA-15 and SBA-16 [5–9]. Studies have been reported on the

* Corresponding author. Tel.: +82 2 880 7438; fax: +82 2 885 6670.
E-mail address: jyi@snu.ac.kr (J. Yi).

0920-5861/$ – see front matter © 2004 Elsevier B.V. All rights reserved.
doi:10.1016/j.cattod.2004.03.070

application of mesoporous materials, especially SBA-15, for use as adsorbents, catalysts and catalytic supports, because of their high surface area, uniformity in pore size and thermal stability [10–14]. However, SBA-16 has not been extensively studied. This is probably due to difficulties encountered in the synthesis and especially in the characterization of this material. A general problem associated with a cubic system is the difficulty in assessing the wall thickness in a simple way. Fortunately, following a procedure used to estimate the wall thickness of MCM-48, recently a very simple way to calculate the wall thickness has recently been published for the cubic *Im3m* structure of SBA-16 [15,16].

Ni catalysts have been used in a variety of catalytic processes such as hydrodesulfurization (HDS) and hydrodechlorination (HDC). More recently, the use of Ni/SiO2 catalysts for use in HDC has been widely studied, because Ni is inexpensive and active in the reaction. However relatively few papers have been published on applications of nickel inside mesoporous materials [14]. The most widely used method for preparing these catalysts is the use of an incipient wetness impregnation process using solutions of simple nickel precursors [17], such as nickel nitrate [18]. Other methods reported for preparing mesoporous silica, MCM-41, supported nickel catalysts include ion-exchange with $NiCl_2$ from $Ni(NH_3)_4(NO_3)_2$ solutions, and direct Ni^{2+} incorporation during the fabrication of the support using a sol–gel method. Nickel loadings are typically low (less than 5 wt.%) [19]. In this study, by adding Ni^{2+} ions into the preparation solution, a strong interaction occurs between the surfactant head group (polyethylene oxide, PEO), Ni^{2+}, and the silica precursors (tetraethoxysilane, TEOS). PEO becomes exposed to the mesopore of mesoporous silica, SBA-16. Finally, Ni becomes located in the mesopore after removal of the structure-directing agent (SDA). Using this approach, nickel catalysts supported on SBA-16 were prepared and compared with SBA-15 catalysts prepared via a single-step procedure. The prepared catalysts were characterized by BET, small angle X-ray scattering (SAXS), X-ray diffraction (XRD), transmission electron microscopy (TEM), inductive coupled plasma (ICP-AES), extended X-ray absorption fine structure (EXAFS) and temperature-programmed reduction (TPR). Catalytic performance was evaluated for the prepared catalyst using the HDC of 1,1,2-trichloroethane to give the vinyl chloride monomer.

2. Experimental

2.1. Catalyst preparation

2.1.1. Ni single-step SBA-15 and SBA-16

Nickel single-step SBA-15 and SBA-16 were prepared using TEOS (Aldrich Chemical Co.) and a nickel nitrate solution, $Ni(NO_3)_2{\cdot}6H_2O$ (Aldrich Chemical Co.) as silica and nickel precursors, respectively. A triblock polymer, poly(-ethyleneoxide)–poly(propyleneoxide)–poly(ethyleneoxide) (EO–PO–EO) was used as a templating agent. Typically, 10 g of Pluonic P123 for Ni-S-15 and 4.7 g of F127 for Ni-S-16 were each dispersed in 322 g of double-distilled water. The resulting solutions were mixed with 52 g of 2 M HCl solution. Finally, 21 g of nickel nitrate and 20.5 g of TEOS were added to the each homogeneous solution with stirring to form a reactive gel. The mixtures were stirred at 40 °C for 20 h. After heating at 100 °C for 24 h, the resulting solids were isolated by filtration and washed. The catalysts were calcined at 450 °C for 5 h in an air.

2.1.2. Ni-supported catalyst

Nickel of 5 wt.% wetness impregnation, SBA-15, and 5 wt.% nickel wetness impregnation SiO_2 were prepared by the wet impregnation of SBA-15, and SiO_2 (Aerosil 200, surface area = 200 m^2/g, pore volume = 3.8 ml/g) with the appropriate amounts of an aqueous solution of nickel nitrate ($Ni(NO_3)_2{\cdot}6H_2O$, Aldrich). After drying at 100 °C for 2 h, the catalysts were calcined at 450 °C for 5 h in air. The prepared catalysts are referred to as Ni-x-y, where x represents the preparation scheme and y denotes the silica support. For example, Ni-I-A indicates that the Ni loading on the aerosil was 5 wt.% via the incipient wetness impregnation technique. The prepared catalyst name and methods can be found in Table 1.

Table 1
Characteristics of the prepared catalysts

Name	Ni (wt %)	Support	Preparation method	D_p (nm)	V_p (m^3/g)	A_p (cm^2/g)	V_m (m^3/g)	S_n[a] (nm)	d_{100} (nm)
SBA-15	–	SBA-15	–	7.8	1.11	812.3		–	8.409
Ni-S-15	5	SBA-15	Single step	6.6	0.81	831.3	0.09	4.1	8.504
Ni-I-15	5	SBA-15	IWI[b]	7.2	0.98	692.8	0.04	8.4	8.409
Ni-I-A	5	Aerosil200	IWI[b]	–	1.38	188.4		10.1	–
SBA-16	–	SBA-16	–	4.5	0.43	713.3	0.15	–	10.56
Ni-S-16	5	SBA-16	Single step	4.5	0.46	888.0	0.24	2.2	10.56
Ni-I-16	5	SBA-16	IWI[b]	4.5	0.38	209.1	0.12	4.2	10.82

D_p: pore diameter; V_p: total pore volume; A_p: BET surface area; V_m: micropore volume; S_n: size of nickel particle; IWI: incipient wetness impregnation.
[a] Particle size is estimated by sherrer equation.
[b] Incipient wetness impregnation.

2.2. Characterization

N_2 adsorption–desorption isotherms were measured using Brunauer–Emmett–Teller equipment (BET; ASAP 2010, Micrometrics) by the static method. Small-angle X-ray scattering (SAXS) patterns were collected on a Bruker GADDS diffractometer using Cu K_α radiation at 40.0 kV and 45.0 mA. The metal composition was measured using inductively coupled plasma-atomic emission spectrometry (ICP-AES; Shimazu ICPS-1000 IV). Powder X-ray diffraction (XRD) patterns of the samples were obtained with a Siemens D5000 diffractometer using a nickel-filtered Cu K_α radiation. The crystalline phases were identified using the Joint Committee on Powder Diffraction Standards (JCPDS) The 2θ angles (with the relative intensities in parentheses), taken from the JCPDS files, are as follows: 37.29 (1 0 1), 43.30 (1 0 0) and 62.91 (1 1 0) for the NiO phase. Extended X-ray absorption fine structure (EXAFS) spectra of Ni/SiO_2 catalysts were obtained on 7C1 EC of Pohang Acceleration Laboratory (PAL) in Korea. The storage ring was operated with an electron energy of 2.5 GeV and a current between 250 and 360 mA. EXAFS spectra at the Ni K-edge were measured in the transmission mode using tow ionization chambers. The energy was scanned in 2 eV steps from 8200–9200 eV. Transmission electron microscopy (TEM) images were collected on a JEM-2000EXII. The samples were reduced by temperature programmed reduction (TPR) from room temperature to 900 °C, at a ramping rate of 10 °C/min, in a flow of 10% H_2 in nitrogen at atmospheric pressure. The flow rate of the H_2/N_2 reducing gas was H_2 = 2 ml/min and N_2 = 20 ml/min for every 0.1 g of catalyst.

2.3. Hydrodechlorination of 1,1,2-trichloroethane

The hydrodechlorination (HDC) of 1,1,2-trichloroethane to the vinyl chloride monomer (VCM) was carried out in a continuous fixed bed reactor (i.d. = 1.0 cm) at atmospheric pressure. The prepared catalyst were charged in a tubular quartz reactor and activated in a stream of hydrogen (20 ml/min) and a helium carrier (20 ml/min) at 400 °C for 2 h and then reduced to the reaction temperature (300 °C). The reactant was fed by a Cole–Palmer syringe pump into the reactor. The exit flow from the reactor after the reaction was passed through an alkali solution trap to adsorb the HCl produced in the reaction. GC-MS and GC (HP 5890 gas chromatography) analysis were carried out to determine the product distribution of the HDC reaction (Table 2).

3. Results and discussion

The Ni content of material prepared via single-step sol–gel processing was estimated to be 5 wt.% by ICP-AES. From this result, comparison catalysts via wetness impregnation of 5 wt.% Ni were also prepared.

3.1. Pore-structure of nickel single-step SBA-15 and SBA-16

The conservation of the mesoporous structure during the single-step processing and calcination stages is important [20]. Fig. 1(A) shows the N_2 adsorption–desorption isotherms for catalyst supported on SBA-15 after calcination. The results showed a type IV isotherm with H1 hysterisis and the characteristics of a material with uniform meso-scale porosity. Fig. 1(B) also shows that the typical N_2 adsorption–desorption hysterisis exists above a relative pressure of 0.45 and a cage like structure for the SBA-16 supported catalyst. When the catalyst is prepared by single-step method, the surface area increases with metal loading (Ni-S-15 = 831.3 m^2/g, Ni-S-16 = 888.0 m^2/g) but the surface area of the wetness impregnation catalyst decreased to 692.8 m^2/g for Ni-I-15 and to 472.6 m^2/g for Ni-I-16. A Relatively high micropore volume ratio to total pore volume (Ni-S-15 = 0.096 and SBA-15 = 0.038, the micropore

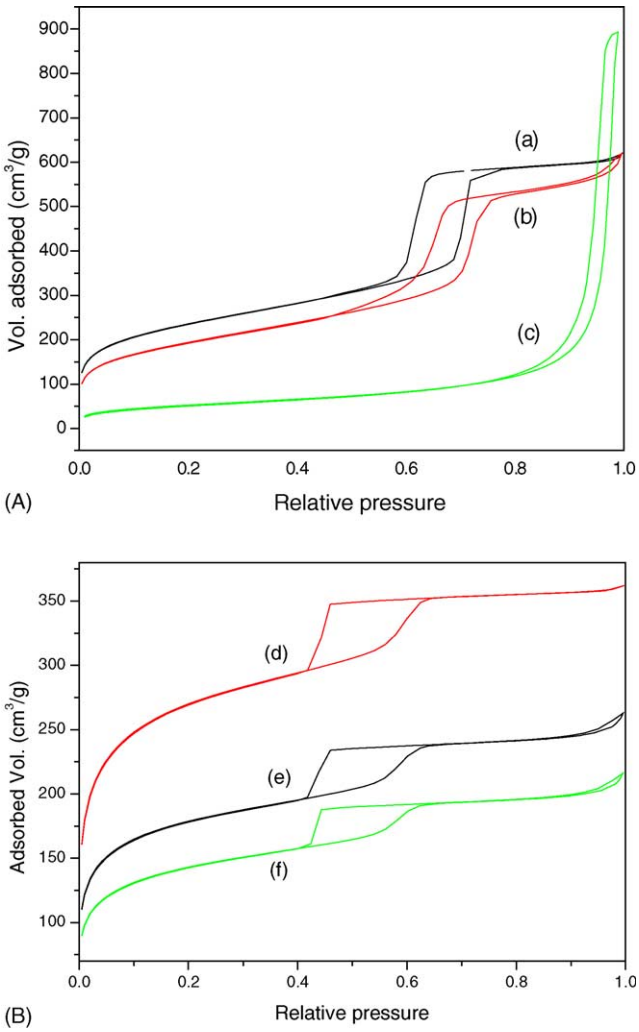

Fig. 1. N_2 sorption isotherm data: (A) catalysts supported on SBA-15 and (B) SBA-16 for (a) Ni-S-15, (b) Ni-I-15, (c) Ni-I-A, (d) SBA-16, (e) Ni-S-16, and (f) Ni-I-16.

volume was estimated by the *t*-plot method.) of Ni-S-15 is probably responsible for this result. The micropore volume ratio, 0.429, of Ni-S-16 is higher than the 0.333 of SBA-16. The micropores originate from the penetration of the EO chains of the triblock copolymer (Pluronic P123 and F127) in the silica walls, thus creating an intrawall porosity, connecting the different mesoporous pores. During the initial stages an interaction among the nickel, the surfactant and the silica source also occurs in acidic conditions, and involves the Ni ion, the positively charged surfactant, and silicate species, such as $(EO)–(H_3O)^+–Cl^-(Si–O)^+$, $(EO–Ni^{++})–(H_3O)^+–Cl^-(Si–O)^+$, and $(EO)–(Ni)^+–Cl^-(Si–O)^+$. The interaction, combined with the increased rate of hydrolysis and condensation of the TEOS at higher temperatures, leads to the formation of an amorphous structure. When the aging temperature is increased ($\geq$80 °C), the EO chains will become more hydrophobic and withdraw inside the hydrophobic PO core, leaving holes in the silica walls [15]. These holes are too unstable to resist the calcination for the removal of SDA. Therefore, the creation of intra wall porosity for single-step catalysts with EO–Ni bonds is enhanced compared to SBA-15 with only EO chains [15,16]. Pore size distribution data (Fig. 2) revealed that Ni-S-15 and Ni-S-16 have virtually identical pore diameters (7.5 nm and 4.5 nm). The relatively small pore diameter of the single-step catalysts supports the view that NiO is located inside of the pores after calcination. The pore diameter, 5 nm, for SBA-16 is smaller than the 7 nm for SBA-15. It is noteworthy that the ratio of micropores to total pores approaches 33%. As mentioned previously, the micropore originates from the penetration of the EO chains of the triblock copolymer, Pluronic F127 ($EO_{106}PO_{70}EO_{106}$), in the silica walls, and the length of the ethylene oxide group of SBA-16 is larger than that for SBA-15. This tendency also follows for Ni-S-15 and Ni-S-16. While the micro volume ratio of Ni-I-16 decreases, some NiO probably becomes located on the micropore after calcination.

The SAXS patterns of prepared catalysts are shown in Fig. 3. The SAXS patterns of the catalyst supported on SBA-15 shows a strong (1 0 0) reflection (2θ = 0.90) and (2θ = 0.91). Three well-resolved peaks in the $2\theta = 0.90^\circ$ and 0.91° regions and two small peaks around 1.5°–1.9° are observed.

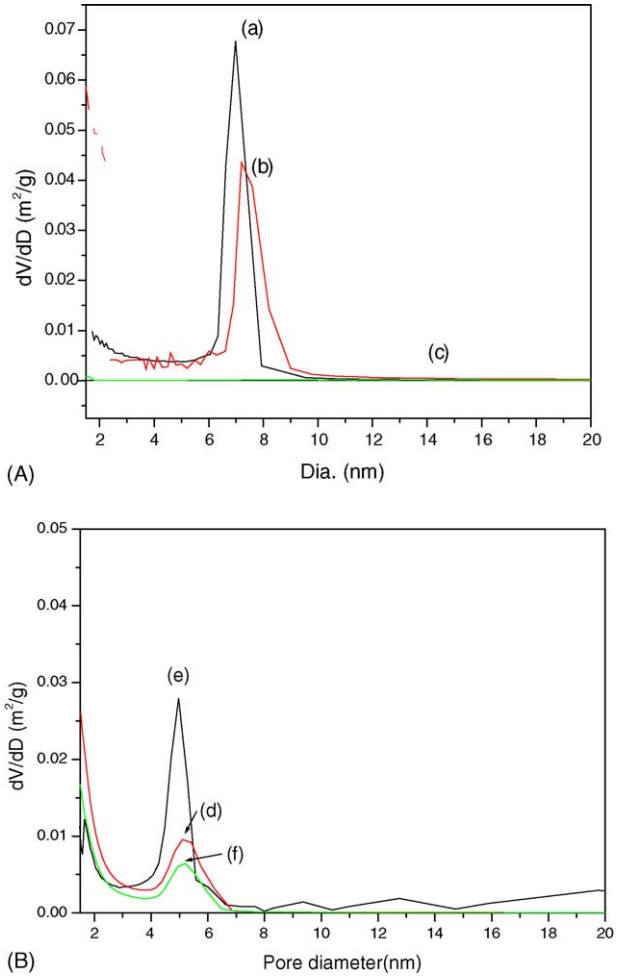

Fig. 2. N_2 sorption isotherm data, pore size distribution: (A) catalysts supported on SBA-15 and (B) SBA-16 for (a) Ni-S-15, (b) Ni-I-15, (c) Ni-I-A, (d) SBA-16, (e) Ni-S-16, and (f) Ni-I-16.

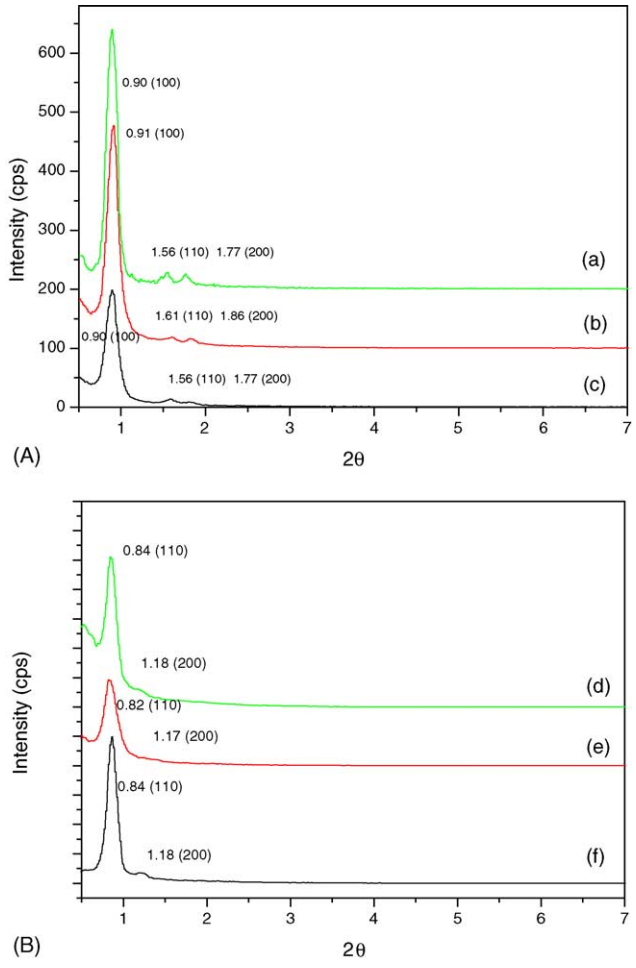

Fig. 3. SAXS patterns of the calcined catalysts: (A) catalysts supported on SBA-15 and (B) SBA-16 for (a) SBA-15, (b) Ni-S-15, (c) Ni-I-15, (d) SBA-16, (e) Ni-S-16, and (f) Ni-I-16.

These, which are assigned as the (1 0 0), (1 1 0), and (2 0 0) reflections of a 2D hexagonal structure, *P6mm*, phase. While a very strong (1 1 0) refection (0.84° 2θ) of the cubic *Im3m* structure and a small shoulder of the (2 0 0) reflection (1.12° 2θ) are detected in catalysts supported on SBA-16. The cell parameter of catalysts supported on SBA-16 is larger than for SBA-15 type catalysts. This tendency is connected to the wall thickness of the samples. In the case of Ni-S-16, the wall thickness of the prepared sample, Fig. 3, was especially calculated to be 5 nm. This indicates that the average wall thickness (4.5 nm) is around the same magnitude as the pore diameter, both having a value slightly above 5 nm. The cell parameter and d_{100} spacing values are shown in Table 1. A decrease in reflections at lower 2θ (SAXS) for catalyst Ni-I-15 and Ni-I-16 was observed. It has a lower long-range order than the others, as reported previously [14,21] that the support structure is partially collapsed or destroyed after introducing the nickel salt by the incipient wetness method. The considerable decrease in the surface area of the impregnated sample, Ni-I-15, can also be attributed to either the loss of crystallites or pore blockage, which can be observed in the TEM image (Fig. 4). The image of Ni-S-15 shows a hexagonal mesoporous structure and regular size nickel particles distributed throughout the pores, and a

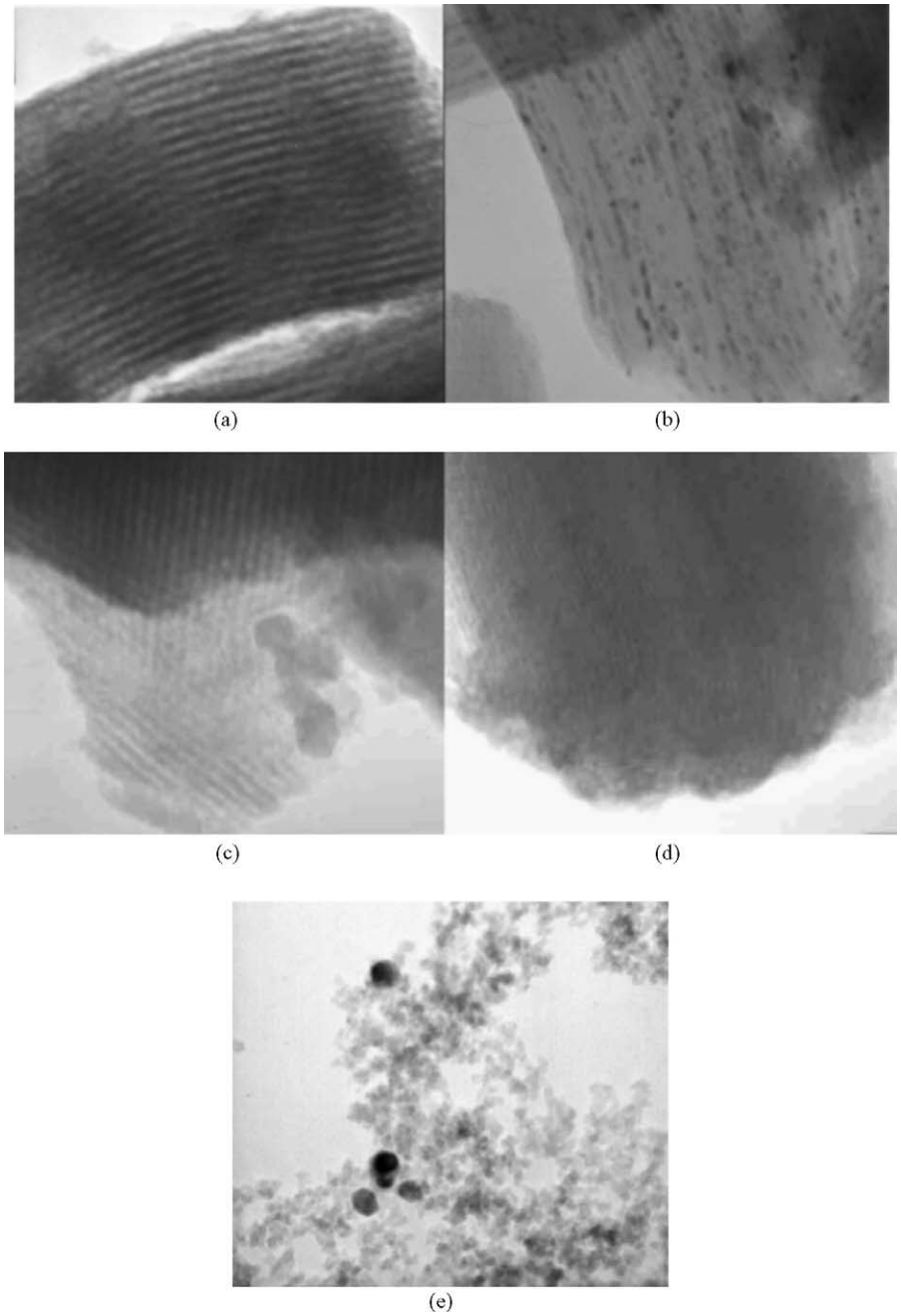

Fig. 4. TEM image: (a) Ni-S-15, (b) Ni-I-15, (c) Ni-S-16, (d) Ni-I-16, and (e) Ni-I-A.

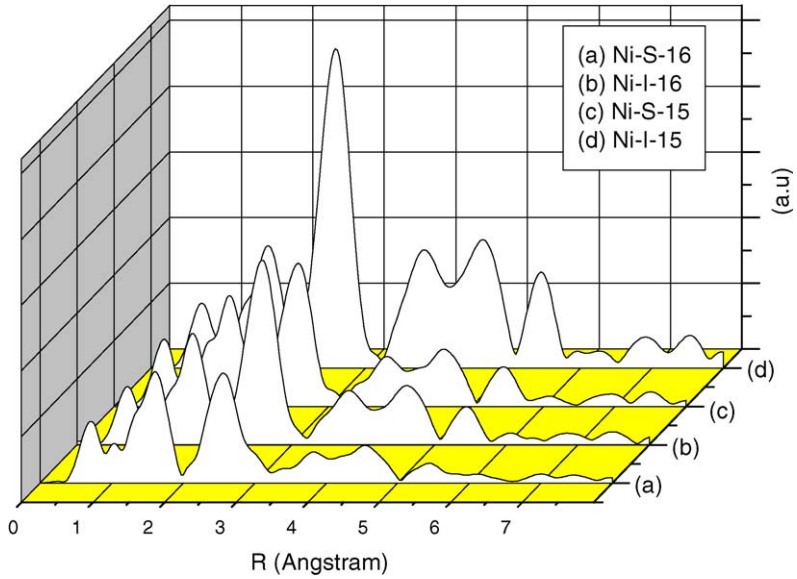

Fig. 5. Radial structure function of calcined catalysts at Ni K-edge: (a) Ni-S-16, (b) Ni-I-16, (c) Ni-S-15, and (d) Ni-I-15.

connected pore structure is shown for Ni-S-16. While Ni-I-15 and Ni-I-16 have various nickel particle sizes and a silica framework, TEM data for Ni-I-A show an irregular pore system and Ni particles.

The radial structure function (RSF) of the EXAFS spectra is also another directive technique for estimating particle size. RSF data for the prepared catalysts after calcination is shown in Fig. 5. The first peak around 2.0 Å can be attributed to the interaction of $Ni(NO_3)_2xH_2O$ (where, x = 4 or 2). While the second-shell interaction around 3.0 Å can be assigned to the mixed interaction of Ni–O and Ni–Ni bonds (Ni–O–Ni interaction) [22,23]. The second shell interaction for catalyst supported on SBA-15 is higher than that for SBA-16, indicating that the nickel particle size on SBA-15 is smaller than that on SBA-16. The catalyst prepared by single-step method's shell interaction is small than the other.

In order to characterize the crystal structure of NiO, XRD measurements were performed on the calcined catalysts (Fig. 6). The XRD pattern of the catalyst after calcination showed a similar peak at 2θ = 37°, 43°, 62°, 72°, and 79°, which are characteristic of NiO (1 0 1), NiO (1 0 2), NiO (1 1 0), NiO (1 1 3) and NiO (2 0 2), respectively. The particle size as estimated from XRD data are listed in Table 1. When the metal is finely dispersed in nano-size particles (less than 3 nm), it should be noted that the characteristic peak is not present. Thus the peak sharpness and intensity are decreased with decreasing metal size. Based on this tendency, the size of the nickel particles for Ni-S-16 and Ni-

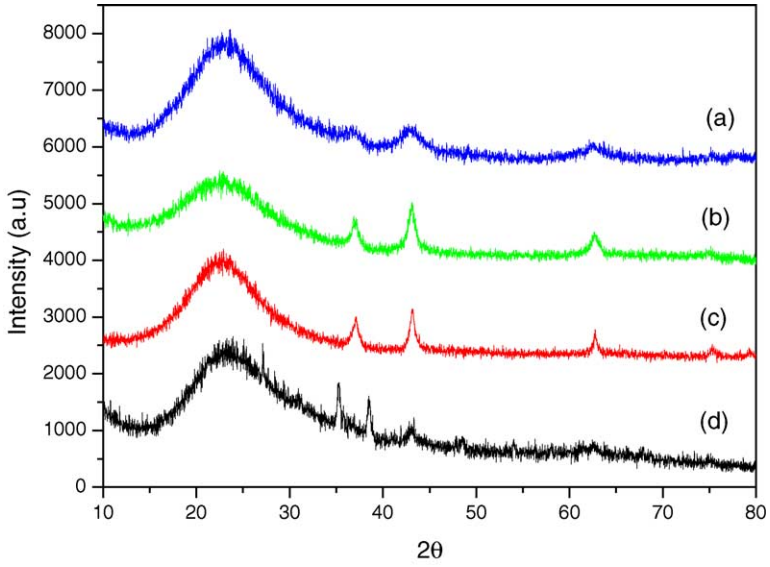

Fig. 6. XRD patterns of calcined catalysts: (a) Ni-S-16, (b) Ni-I-16, (c) Ni-S-15, and (d) Ni-I-15.

Table 2
Flow reactor experimental conditions

Catalyst reduction	
Temperature (°C)	400
H_2 in N_2 flow rate (ml/min)	40
Time (h)	2
HDC reaction	
Temperature (°C)	300
Weight hourly space velocity (g-cat h/mol)	13.34
Catalysts weight (g)	0.1

I-16 is smaller than that for Ni-S-16 and Ni-I-16. The cage like structure and large portion of micropores probably leads to this result at the same metal content, 5 wt.%. When the catalyst is reduced the specific peak is more broad.

TPR experiments were performed to investigate the reduction of the NiO particles in the prepared catalysts (Fig. 7). Mile et al. [20] reported that bulk NiO, when attached to silica can be reduced at 300–400 °C and 400–500 °C, respectively. In the Ni-S-15 and Ni-S-16 catalysts, prepared by the single-step method, a large reduction peak at lower temperatures (350–400 °C) was observed. This peak is believed to be due to NiO reduction in the main mesopore of the SBA-15 while a broad high temperature peak (500–700 °C) for Ni-I-15 and Ni-I-16 catalysts, prepared by the incipient wetness technique, was mainly observed. A larger portion of high temperature peak was found for Ni-I-16. This indicates that loaded Ni is probably located in the micropores, the micropore therefore decrease from 0.333 of SBA-16 to 0.313. In post-hydrothermal treatment catalysts (Ni-I-15 and Ni-I-16), a high temperature peak is normally observed when samples are prepared by incipient wetness technique and dried at 100 °C. Their formation is probably the result of a condensation reaction between the OH– groups of the silica with the metal nitrate salts upon heating and those of the silica surface [24–26]. Other authors have reported that nickel hydrosilicate is formed in Ni catalysts supported on silica, which are prepared by incipient wetness [22,25,26]. From the single-step preparation scheme, which does not involve a post hydrothermal treatment, it can be concluded that a regular size of NiO was formed on the silica surface.

3.2. Hydrodechlorination of 1,1,2-trichloroethane into vinyl chloride monomer

The reaction products consisted of vinyl chloride monomer (VCM), dichloroethane, methane, ethylene and 1,1,2-TCEa, based on GC-MS results. A proposed scheme for the selective HDC of 1,1,2-TCEa into VCM over Ni/SiO_2 catalysts is as follows [14,25]:

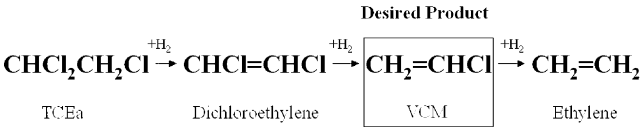

Catalysts supported on SBA-16 show particularly high conversion and high selectivity with respect to the VCM in the HDC of 1,1,2-TCEa (Fig. 8). The initial activity of most catalysts was about 90%, however the conversion on Ni-I-15 was low, about 75%. After 10 h (steady state), however, the 40% value for Ni-I-15 is higher than the approximate 10% conversion for Ni-I-15. Based on the conversion data, the most active catalyst is Ni-S-16 through the reaction time. When the nickel is located in a micropore, a high temperature peak is detected in the TPR patterns. The high temperature peak however is not present in Fig. 7. Based on this tendency, loaded nickel appears to mainly exist on the mesopore surface. Most of the micropores, therefore are

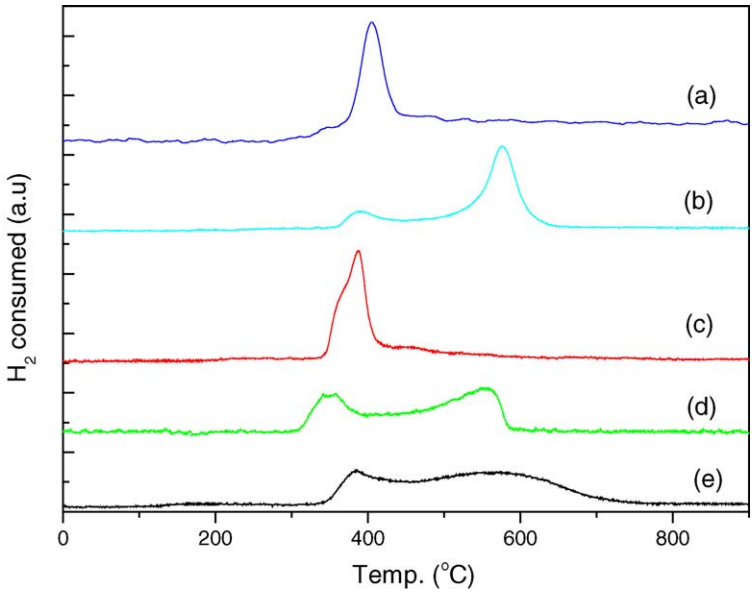

Fig. 7. TPR patterns of calcined catalysts: (a) Ni-S-16, (b) Ni-I-16, (c) Ni-S-15, (d) Ni-I-15, and (e) Ni-I-A.

used as a path for reactant. Consequently, a high conversion of 1,1,2-TCEa is achieved on Ni catalysts supported on SBA-15. While the data for Ni-I-16 (nickel is mainly located on micropores) show a relatively low conversion and VCM selectivity. The initial conversion over Ni-I-A is high but the steady state conversion is lower than the others, since nickel hydrosilicate has some effect on the stability of the catalyst but the active site is reduced and the catalytic activity is decreased [25,26]. Due to the irregular size of nickel particles and the low surface area (N_2 adsorption–desorption isotherm and TEM), the rate of deactivation of Ni-I-A is faster than the others. Based on the TPR results, the characteristic peak area of nickel hydrosilicate at 550 °C is larger than that for bulk nickel oxide at around 400 °C. The high surface area and NiO peak ratio lead to the conclusion that Ni-S-15 and Ni-S-16 showed a higher conversion than Ni-I-15 and Ni-I-16 (the same support, SBA-15, and different preparation method). The partial collapse or destruction of pore structure (TEM and TPR) is possibly one reason for these results. In the case of HDC, the catalytic activity increases proportionally with the nickel atomic group, neighboring nickel atoms and larger metal size. Shin and Keane [27,28] reported that a high catalytic activity is related to a low dispersion of metal in the HDC of chlorobenzene. This pattern is consistent with the initial high conversion, 90%, of Ni-I-A and low conversion, 75%, of S-2. Choi and Lee [25,26] also reported that HCl is formed during the HDC reduction and altered the crystal structure of metallic nickel. In connection with this, Scott et al. [29] proposed that the catalyst deactivation was due to an electron effect between the adsorbed Cl and the metal.

VCM is a reaction intermediate in the HDC of 1,1,2-trichloroethane. Initially, the main products are therefore methane and ethylene. VCM selectivity generally increases as a function of reaction time and decreases at a specific point. In order to increase VCM selectivity, a large ensemble and adsorption site is required [27,28]. Therefore, a fine dispersion condition is more favorable for high VCM selectivity. Tavoularis and Keane [30] reported that the activity of HDC increases with metal size. HDC over the Ni-S-15 and Ni-S-16 catalysts, which have relatively small or regular sized nickel particles, showed a high VCM selectivity, yield, and a steady reaction activity. In particular, the VCM yield also ranged from 55% at the initial point to 20%. From the reaction data, the initial active catalyst (Ni-I-A) is not selective for VCM since its surface is covered by firmly adsorbed hydrogen, compared to the others and the competition of chlorinated compounds with hydrogen for adsorption would be unfavorable. Therefore a complete conversion to the final product (methane or ethylene) occurs. The deactivation rate of a catalyst with a large and irregular size particle is so fast that the initial conversion over Ni-I-A is high but the VCM selectivity is low. Accordingly, a regular sized nickel supported on mesoporous silica could be prepared and steady catalytic activity and high VCM selectivity could be achieved by introducing a noble single-step sol–gel method.

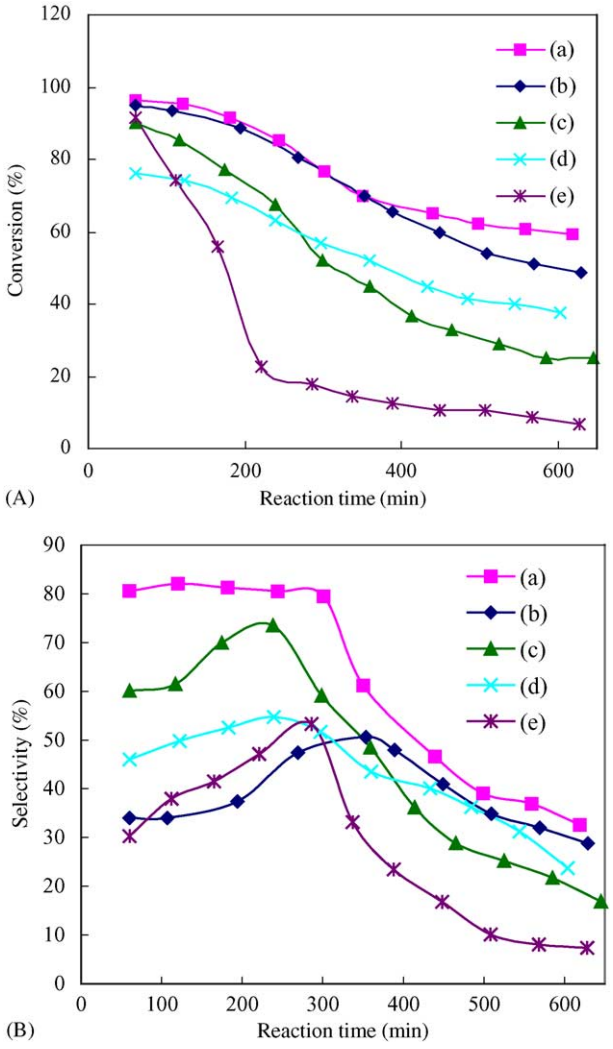

Fig. 8. Catalytic activity (A) and VCM selectivity (B) for the prepared catalysts; (a) Ni-S-16, (b) Ni-I-16, (c) Ni-S-15, (d) Ni-I-15, and (e) Ni-I-A.

4. Conclusions

Nickel catalysts supported on mesoporous silica, SBA-15 and SBA-16, were successfully synthesized via single-step process based on the strong interaction between nickel, silica precursors and micelles in the assembly of SBA-15 and SBA-16. N_2 sorption, SAXS, and TEM images indicated that a large surface area, a pore orderness of 2D hexagonal and 3D cubic structures of the prepared catalyst were conserved throughout the single-step sol–gel procedure in acidic media, but pore blocking and deformation of catalyst structure were found to occur in catalysts prepared by the incipient wetness technique. Based on TEM, XRD, and EXAFS data, a relatively small and regular size nickel particle (2.2 nm) was obtained in the Ni catalyst supported on SBA-16. TPR and TEM showed that relatively small and

regular size nickel particles were mainly present on the mesopore. BET data also indicated a cage like pore structure and high micropore volume ratio. From TPR patterns, the loaded nickel was located on the mesopores in Ni-S-16. Nickel hydrosilicate was formed in the catalyst prepared by the incipient wetness technique as well as for the hydrothermal process. Nickel hydrosilicate and pore deformation are assumed to be the reasons for the low catalytic activity found in the incipient wetness technique. In addition, high VCM selectivity and activities were achieved for the nickel catalyst supported on the SBA-16 prepared for the hydrodechlorination of 1,1,2-TCEa. Using the SBA-16 type support with a 3D cage like, mesopre structure and a high micropore ratio, relatively high conversion could be achieved. Moreover, high VCM selectivity could be obtained on nickel catalysts prepared using the single-step method.

Acknowledgment

This work was supported by NRL (National Research Lab) project of Korea Ministry of Science and Technology and the authors thank PAL (Pohang Acceleerator Lab, Korea) for EXAFS experiment.

References

[1] A. Gampine, D.P. Eyman, J. Catal. 179 (1998) 215.
[2] J. Stach, V. Pekarek, J. Hetflejs, Chemosphere 39 (1999) 2391.
[3] D. Barrialt, M. Sylveste, Can. J. Microbiol. 39 (1993) 593.
[4] M. Trillas, J. Peral, X. Domenech, J. Chem. Technol. Biothechnol. 67 (1996) 237.
[5] D.J. Moon, M.H. Chung, K.Y. Park, S.I. Hong, Appl. Catal. A 168 (1998) 159.
[6] D. Zhao, J. Feng, Q. Huo, N. Melosh, G.H. Fredrickson, B.F. Chmelka, G.D. Stucky, Science 279 (1998) 548.
[7] P. Yang, D. Znao, D.I. Margolese, B.F. Chemelka, G.D. Sucky, Nature 396 (1998) 152.
[8] G. Attard, J.C. Glyde, C.G. Göltner, Nature 378 (1995) 366.
[9] S.A. Bagshaw, E. Prouzet, T.J. Pinnavaia, Science 269 (1995) 1242.
[10] J.M. Kim, G.D. Stucky, Chem. Commun. (2000) 1159.
[11] Y. Park, T. Kang, Y.S. Cho, J.C. Park, J. Yi, Stud. Surf. Sci. Catal. 146 (2003) 637.
[12] J.C. Park, J.H. Lee, P. Kim, J. Yi, Stud. Surf. Sci. Catal. 146 (2003) 109.
[13] T. Kang, Y. Park, J.C. Park, Y.S. Cho, J. Yi, Stud. Surf. Sci. Catal. 146 (2003) 527.
[14] Y.S. Cho, J.C. Park, B. Lee, Y. Kim, J. Yi, Catal. Lett. 81 (1/2) (2002) 89.
[15] P. Van Der Voort, M. Benjelloun, E.F. Vansant, J. Phys. Chem. B 106 (35) (2002) 9027.
[16] K. Morishige, N. Tateishi, S. Fukuma, J. Phys. Chem. B 107 (22) (2003) 5177.
[17] D.J. Lensveld, J.G. Mesu, A.J. van Dillen, K.P. de Jong, Microporous Mesoporous Mater. 44/45 (2001) 401.
[18] T. Halachev, R. Nava, L. Dimitrov, Appl. Catal. 153 (1995) 25.
[19] U. Junges, S. Disser, G. Schmid, F. Schmid, F. Schüth, Stud. Surf. Sci. Catal. 117 (1998) 391.
[20] B. Mile, D. Stirling, M.A. Zammitt, A. Lovell, M.J. Webb, J. Catal. 114 (1998) 217.
[21] Y. Park, T. Kang, Y. Cho, P. Kim, J. Park, J. Yi, Stud. Surf. Sci. Catal. 146 (2003) 637.
[22] J.C. Yang, Y.G. Shul, C. Louis, M.M. Che, Catal. Today 44 (1998) 315.
[23] C. Louis, Z.X. Cheng, M. Che, J. Phys. Chem. 97 (1993) 5703.
[24] A. Roman, B. Delmon, J. Catal. 30 (1973) 333.
[25] Y.H. Choi, W.Y. Lee, Catal. Lett. 67 (2000) 155.
[26] Y.H. Choi, W.Y. Lee, J. Mol. Cat. A: Chem. 3184 (2001) 1.
[27] E.J. Shin, M.A. Keane, Catal. Lett. 58 (1999) 141.
[28] E.J. Shin, M.A. Keane, Appl. Catal. B 18 (1998) 241.
[29] S.P. Scott, T.J. Sweetman, A.G. Fizgerald, E.J. Strurrock, J. Catal. 168 (1998) 501.
[30] G. Tavoularis, M.A. Keane, J. Mol. Catal. A 142 (1999) 187.